Vibrational Spectroscopy 101 (2019) 52–63

Contents lists available at ScienceDirect

Vibrational Spectroscopy

journal homepage: www.elsevier.com/locate/vibspec

Fundamental infrared absorption features of α-quartz: An unpolarized single-crystal absorption infrared spectroscopic study

Mingyue He[a], Wei Yan[a,b,c], Yedi Chang[d], Kexin Liu[d], Xi Liu[b,c,*]

[a] School of Gemmology, China University of Geosciences (Beijing), Beijing, 100083, China
[b] School of Earth and Space Sciences, Peking University, Beijing, 100871, China
[c] Key Laboratory of Orogenic Belts and Crustal Evolution, Ministry of Education of China, Beijing, 100871, China
[d] School of Physics and State Key Laboratory of Nuclear Physics and Technology, Peking University, Beijing, 100871, China

ARTICLE INFO

Keywords:
α-Quartz
Fundamental IR modes
Interference fringes
IR absorption features
Sample thickness

ABSTRACT

With an unpolarized light normally directed to three α-quartz crystal plates cut perpendicularly (Z-cut) or parallel to the optical axis (X-cut and Y-cut), single-crystal absorption infrared spectra from ~1300 to 50 cm^{-1} were measured. To obtain optimal results, thin sections with different thicknesses (~100, 50, 20 and 6 μm) were prepared and probed. On the basis of symmetry analysis and pertinent knowledge in the literature, the effect of possible interference in the absorbance spectra was evaluated and tentatively removed, and optimal spectroscopic results (peak position, peak intensity, and peak width) were obtained for the fundamental IR-active modes of α-quartz, including all four A_2 modes and seven E modes. In particular, the present contribution directly observed those extremely strong light-absorbing IR peaks in the ~1300–1000 cm^{-1} region, which had not been experimentally detected before. Supplementary Raman data were collected from these well-polished crystal plates. Our exercise eventually led to a full description of the vibrational features of α-quartz. The full characterization of the vibrational properties of α-quartz should shed lights on better understanding of the structural and vibrational features of α-quartz, its polymorphs, vitreous silica, and even other silicate minerals.

1. Introduction

α-Quartz (low-temperature quartz) is the second most ubiquitous mineral in the Earth's crust [1], appearing in igneous, sedimentary and metamorphic rocks [2]. It is also present in various meteorites, and lunar and Martian rocks [3]. Its physical and chemical properties, vibrational properties included, are therefore essential for many geological and planetary investigations. The great interest concerning its infrared (IR) features is based on two important aspects. First, vibrational spectroscopy succeeds in shedding unique lights into not only structural features [4–6] but also many crucial physical properties relevant to Earth science, such as the thermodynamics and elastic properties [6–12]. Second, this mineral represents a physical system where both anisotropy of the short-range forces and transverse optic (TO)-longitudinal optic (LO) splitting induced by the long-range Coulomb interactions exist [13,14], and all of the vibrational modes are active at the Brillouin zone center [15], so that it traditionally serves as an important benchmark system for testing the accuracy of the theories in reproducing the lattice vibrations of other silicates. It adopts a three-dimensional framework structure in which all constituent SiO_4 tetrahedra are corner-sharing [16], a phenomenon prevalent in many SiO_2 polymorphs, vitreous silica [17], and other more complex silicate minerals. As such, it has been the target of many experimental [13,18–25] and theoretical investigations [14,26–33].

There have been many experimental studies about the IR features of α-quartz. The employed experimental techniques included powder IR spectroscopy, single-crystal reflection, absorption and emission IR spectroscopy [18–25,34–37]. The powder method, mixing the target material with KBr (or similar IR-inactive substances) into a fine-grained powder, pressing the powder into a clear and transparent pellet, and analyzing the pellet with transmitting IR light, is a rapid and convenient technique. However, this method suffers unavoidable atmospheric water contamination [38], complicated scattering effects [39], polarization effects [23,37], rounding of intense peaks [40], confusing relative peak heights [6], and incompetence of discerning the TO and LO components. Additionally, assigning the IR peaks to certain symmetry species can only be undertaken by analogy with the frequencies revealed by other approaches, which may lead to many uncertainties and even mistakes. The single-crystal reflectance IR spectroscopy method also requires a minimum amount of sample preparation (polishing a

* Corresponding author at: School of Earth and Space Sciences, Peking University, Beijing, 100871, China.
E-mail address: xi.liu@pku.edu.cn (X. Liu).

https://doi.org/10.1016/j.vibspec.2019.02.003
Received 30 December 2018; Received in revised form 29 January 2019; Accepted 1 February 2019
Available online 05 February 2019

crystal facet of the target material), and is capable of recognizing the TO-LO splitting (particularly sensitive to the LO components) [41]. Its major drawback is that the reflection spectra are distorted and hard to analyze [43]. The reflection data, for instance, does not directly constrain the TO and LO frequencies, and complicated analytical methods such as the dispersion analysis and Kramers-Kronig analysis have to be employed [19,21,43–45]. The single-crystal transmission IR technique has an extremely demanding sample-preparation procedure, requiring making parallel-sided, stand-alone, doubly-polished thin sections with thicknesses of usually a few microns only [46–48]. As long as the sample can be properly prepared, however, this technique can straightforwardly determine the intrinsic IR features in general, and directly derive the TO and LO frequencies in particular (highly sensitive to the TO components) [49]. The single-crystal emission IR technique has some special requirements on the instrumentation and data-analyzing process, and has not been widely used so far [25,50,51]. Despite all the efforts, the fundamental infrared absorption features of α-quartz are still poorly constrained. Until now, all the absorbance data were collected from very thick samples (e.g. a minimum sample thickness of ~31 μm in Saksena [34] and a sample thickness of ~25 μm in Kats [18]), which did not allow any light in the energy range of ~1350–950 cm^{-1} to pass through. The thus-obtained IR peaks are likely erroneous hence. According to some recent contributions to the IR absorbance features of silicates such as olivine and coesite [48,52], thin sections with thicknesses down to a few microns must be used in order to obtain correct IR absorbance data for the Si-O stretching vibrational modes.

Theoretical methods have been applied to constrain the IR characteristics of α-quartz as well. They can be divided into two major families, one using an empirical force field approach with its results relying on the used force fields or potentials [14,15,26–28,53,54], and the other using more sophisticated density-functional theory [29–32,55]. In these simulations, the experimental IR data were usually taken as critical references, and enormous efforts were made to reproduce these experimental results. Due to the fore-mentioned uncertainties in the experimental data, the theoretical results could not be completely problem-free.

In addition to the IR spectra, Raman spectra have also been acquired, which can provide important clues to the IR features of α-quartz, particularly to those fundamental vibration modes which are both infrared-active and Raman-active [13,56–58].

The present work has been undertaken with the main aim of providing a more convincing and comprehensive account of the fundamental IR absorbance features of α-quartz in both mid- and far-IR regions. To achieve this goal, we performed single-crystal transmission mid- and far-IR measurements on some crystallographically-orientated thin sections cut from a natural, clear, euhedral α-quartz crystal. We collected data from thin sections of different thicknesses (from ~100 to 6 μm), so that the IR vibrational modes with different light-absorbing capabilities could be confidently observed. Complementarily, we also collected unpolarized Raman spectra from some of the thin sections.

2. Experimental and analytical methods

2.1. Thin section preparation

A natural, clear and euhedral α-quartz prism (~29 mm in height and ~13 mm in diameter) from Donghai County of Jiangsu Province (China) was used in this study. It had no discernable cracks, and no visible mineral inclusions or fluid inclusions. Its perfect morphology made its crystallographic orientations easily-determined, enabling us to prepare thin sections along particular crystallographic orientations. In total, three thin sections with different orientations were prepared: (1) crystal plate cut perpendicularly to the optical axis (//(001); Z-cut), (2) crystal plate cut parallel to one of the three 2-fold axes (a_1, a_2 and a_3) and the optical axis (//(100); X-cut), and (3) crystal plate cut perpendicularly to one of the three 2-fold axes and the optical axis (//(010); Y-cut), as shown schematically in Fig. 1.

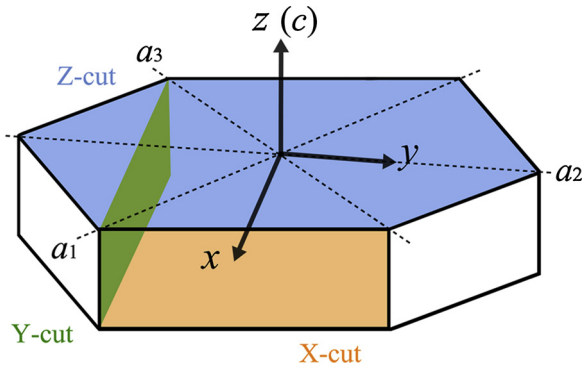

Fig. 1. Schematic diagram showing the crystallographic orientations of the thin sections cut from our natural α-quartz, with the plane (001) in blue standing for the Z-cut sample, the plane (100) in orange for the X-cut sample, and the plane (010) in green for the Y-cut sample. The c axis is the 3-fold screw axis (i.e. the optical axis or z axis), and the a_1, a_2 and a_3 axes are the three 2-fold axes.

In order to prepare parallel-sided, stand-alone, doubly-polished thin sections for transmission FTIR investigations, the general procedures documented in Liu et al. [47] were followed. The thin sections cut by a low-speed diamond saw were first mounted on glass slides with crystal-bond, and subsequently reduced to the desired thickness by manually grinding and carefully polishing both sides under water with a series of silicon carbide abrasive papers. After removed from the glass slides, the polished thin sections were thoroughly washed in acetone for 30 min to dissolve the crystal-bond, cleaned in ethanol for another 30 min, subsequently dried at ~110 °C in an oven for several hours, and eventually analyzed with the FTIR spectroscopy.

In order to obtain optimal FTIR results, the above sample-mounting, sample-grinding, sample-polishing, sample-washing, sample-drying and sample-analyzing procedure was repeated for several times, leading to acquiring FTIR spectra from all those three thin sections with a series of thicknesses of ~100, 50, 20 and 6 μm. The thicknesses of the thin sections were determined by utilizing a digital micrometer with an accuracy of ± 2 μm [46].

2.2. Mid-IR spectroscopy

Transmission mid-IR spectroscopy measurements at room temperature were conducted using a Nicolet iN10 MX IR Microscope (Fig. 2a), equipped with a high-energy Ever-Gloinfrared source, a standard KBr beam splitter, a liquid-nitrogen-cooled MCT detector [48,52,59]. Unpolarized IR spectra were collected from 4000 to 675 cm^{-1}, with an aperture size of 50 × 50 or 30 × 30 $μm^2$, and with a resolution of 4 cm^{-1}. Up to 512 scans were taken for every analysis. In every individual IR analysis, we analyzed the background first, and the sample afterwards. The IR spectra were processed by using the OMNIC 8.2 software.

2.3. Far-IR spectroscopy

Transmission far-IR spectra at ambient conditions were acquired by operating a Bruker Vertex 80v FTIR spectrometer (Fig. 2b), which was an evacuated optics bench capable of eliminating potential effects of atmospheric moisture [60,61]. The spectrometer was equipped with an externally water-cooled high power Hg-arc source, a 6 μm Mylar Multilayer beam splitter, and a DTGS detector operating at room temperature. No polarizer was employed in the measurements. In each individual analysis, we similarly analyzed the background first, and the sample afterwards. In order to improve the signal-to-noise ratio, a scanning speed of ~2.5 kHz was used, a sample area of 8 × 8 mm^2 was

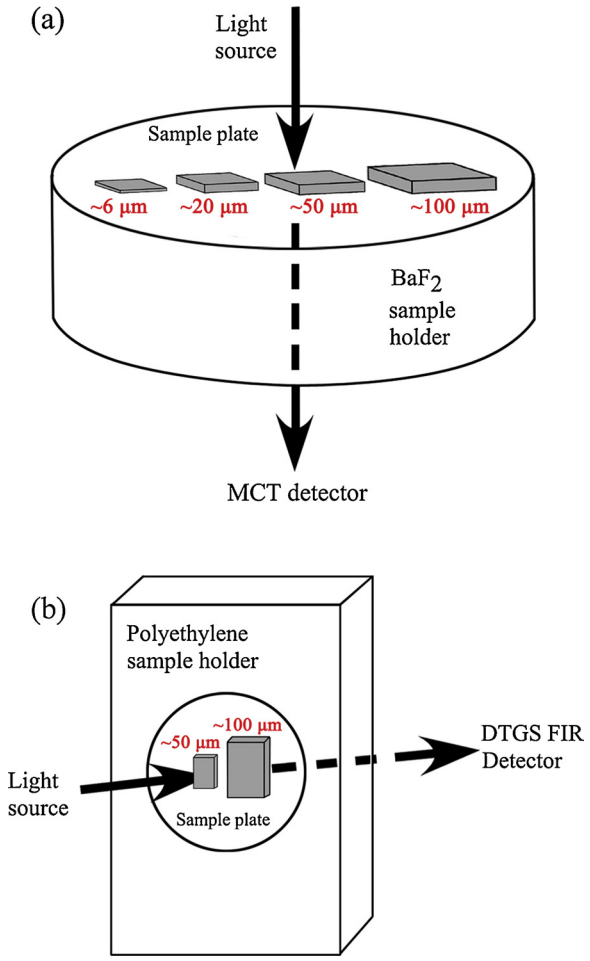

Fig. 2. Schematic setting-up in the transmission mid-IR experiments (a), and in the transmission far-IR experiments (b). In the mid-IR experiments with a Nicolet iN10 MX IR Microscope (a), the incident light from the high-energy Ever-Glo infrared source normally traveled through the sample plate and the BaF_2 sample holder, and subsequently entered the liquid N_2-cooled MCT detector. In the far-IR experiments with the Bruker Vertex 80v FTIR spectrometer (b), the incoming beam of unpolarized light from the externally water-cooled high power Hg-arc source horizontally passed through the sample plate and the polyethylene sample holder, and was finally picked up by the DTGS detector operating at room temperature. Special care was paid in evacuating the instrument in the whole analyzing process, in order to eliminate the significant influence of atmospheric moisture absorptions in the far-IR region. Transmission mid-IR data were collected for all three thin sections with different crystallographic orientations at four different sample thicknesses (~100, 50, 20 and 6 μm) whereas transmission far-IR data were collected for all three thin sections at two different samples thicknesses only (~100 and 50 μm).

probed, and 128 scans were accumulated for every measurement. The spectra were collected from 650 to 50 cm^{-1}, with a spectral resolution of 4 cm^{-1}. We only analyzed the ~100 and 50 μm thick thin sections. The data were processed by the OPUS program.

2.4. Unpolarized Raman spectroscopy

As a supplementary to the IR spectra, unpolarized Raman spectra were collected from 100 to 1350 cm^{-1} with a Renishaw inVia Reflex system in a back-scattering geometry at room *P-T* conditions. The analytical conditions, identical to those reported in Liu et al. [62], were a 532 nm laser, an ~50 mW emission power, a 50× long-distance objective, ~1 μm light spot, 1 cm^{-1} spectral resolution, and an accumulation of 20 successive scans for every analysis (10 s for each scan). The spectra were acquired from well-polished surfaces of the Z-cut, X-cut and Y-cut samples with thicknesses of several hundred microns.

3. Results

We firstly present the theoretical predictions of the fundamental optical vibration modes of α-quartz. We secondly show our unpolarized Raman spectra, which well constrain those both Raman-active and IR-active vibrational modes. We thirdly examine the effects of different sample thicknesses, and fourthly constrain the influence of potential interference fringes on our unpolarized single-crystal transmission IR spectra, aiming for the best quality of the IR features in different energy ranges. We then deconvolute our optimal IR spectra to obtain the fundamental IR modes of α-quartz, and arrive at a full set of band assignments. Finally, a comparison between the present results and those in the existing experimental and theoretical investigations of α-quartz is performed.

3.1. Symmetry analysis and TO-LO splitting

α-quartz has a trigonal symmetry, and appears in two enantiomorphs with respective space groups $P3_121$ (D_3^4) and $P3_221$ (D_3^6) (Z = 3) [63]. Its structure, accordingly, possesses the symmetry elements of a 3-fold screw axis (i.e. the optical axis), and three 2-fold axes separated by 120°. The 3-fold screw axis is normal to all three 2-fold axes (Fig. 1). With nine atoms in the primitive cell, the factor group analysis has suggested that α-quartz has 27 vibrational normal modes, including 4 symmetric modes (A_1), 5 antisymmetric modes (A_2) and 18 doubly degenerate modes (E) [64,65]. Three of the vibrational normal modes are acoustic ($1A_2 + 2E$). The irreducible representation of the optical modes of α-quartz is then

$$\Gamma_{OP} = 4A_1 + 4A_2 + 8E \quad (1)$$

where the A_1 modes are Raman-active, A_2 modes are IR-active, and E modes are both Raman- and IR-active.

The above classification of the optical modes (Eq (1)) is valid only when the macroscopic electric field in the crystal is neglected [14,65]. If this macroscopic electric field is taken into account, the long-range Coulomb interactions will give rise to the TO-LO splitting, so that some reductions of some optical modes will be inevitable, bringing about the splitting of the A_2 and E modes in the case of α-quartz [66]. The magnitude of thesplitting depends on the oscillator strength, being large in the strong absorption regions whereas small in the weak absorption regions [4,67,68]. It has been demonstrated that thesplitting in α-quartz can be as large as ~160 cm^{-1} for the Si-O stretching motions [19,21]. A proper consideration of the TO-LO splitting is therefore critical.

Taking the TO-LO splitting into account, one may then observe all A_1 and E-TO modes as the wave vector propagates along the z direction, and detect all A_1, E-TO and E-LO modes as the wave vector propagates normally to the z direction using unpolarized Raman spectroscopy [14] In comparison, one may observe all A_2-LO and E-TO modes as the wave vector propagates along the z direction, and find all A_2-TO, E-LO and E-TO modes as the wave vector propagates normally to the z direction with unpolarized IR spectroscopy [20].

3.2. Unpolarized Raman features of α-quartz

In general, Raman-active vibrational modes appear as sharp and well-separated peaks in Raman spectrum, and Raman spectroscopy can be used to effectively detect the A_1, E-TO and E-LO modes of α-quartz. The knowledge thus-obtained can then aid in constraining the infrared-active E-TO and E-LO modes.

Raman spectroscopy was applied to α-quartz almost a century ago [69]. Ever since, the Raman features of α-quartz have been well established and their symmetry assignments have been accomplished

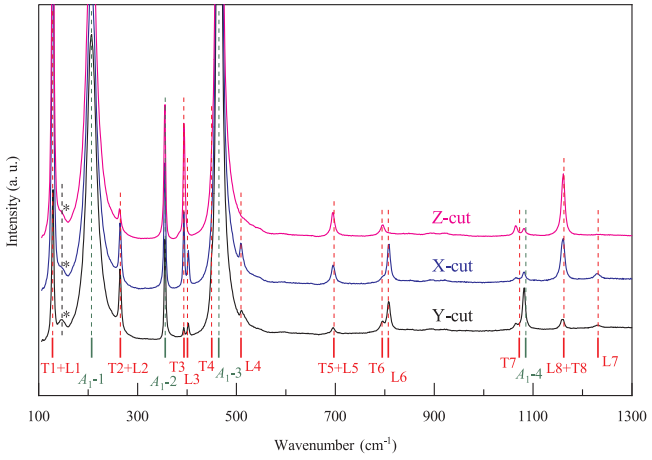

Fig. 3. Unpolarized Raman spectra collected from the Z-cut, X-cut, and Y-cut samples (sample thicknesses being several hundred microns). The Raman feature at ~147 cm^{-1} caused by an anharmonic interaction between a "soft" zone-center optical phonon and an excitation consisting of two oppositely directed zone-edge acoustic phonons (*) [71] is most prominent in the Raman spectrum taken from the Y-cut sample. All other Raman features are attributable as either fundamental A_1 modes (consecutively labeled as A_1-1 to A_1-4) or E modes (consecutively labeled as E1 to E8). Note that for the purpose of saving space, the E modes with the TO and LO components have been further abbreviated, with T1 representing E1-TO for example. As a comparison, the frequencies of the A_1 modes and E modes from Scott and Porto [13] are shown as short thick lines. In most cases, the positions of the Raman peaks observed in this study are in good agreement with those from Scott and Porto [13], but in a few cases, small discrepancies do exist (e.g. the E7-TO and A_1-4 peaks).

[13,56–58,70–72]. In the early experiments, the Raman data was usually acquired on oriented crystal cubes using a forward-scattering technique with polarized incident and scattered radiations. Later on, Raman spectroscopic experiments were performed with unpolarized lights on unoriented grains using either a forward-scattering or back-scattering technique to detect the effects of P, T and grain size on the Raman features [66,73,74]. More recently, Raman spectra were routinely collected with unpolarized lights on unoriented grains in petrographic thin sections using a back-scattering technique for the purpose of identifying phases [75,76]. However, standard Raman spectra collected with unpolarized lights on oriented α-quartz crystals using a back-scattering technique have remained unavailable.

Our Raman spectra collected with unpolarized lights on the Z-cut, X-cut and Y-cut samples using a back-scattering technique are shown in Fig. 3, and the corresponding frequencies and symmetries of the major Raman features are listed in Table 1. Evidently the overall appearances of the Raman spectra from these three thin sections are much comparable. Firstly, all A_1 modes are observed in all Raman spectra at almost identical frequencies, and their peak heights are generally comparable with the only exception of the A_1-4 mode at ~1082 cm^{-1}; the Raman peak at ~1082 cm^{-1} from the Y-cut sample is much stronger than from the Z-cut and X-cut samples. Secondly, four doubly degenerated E species with no observable TO-LO splittings (E1-TO + E1-LO, E2-TO + E2-LO, E5-TO + E5-LO and E8-TO + E8-LO; Fig. 3) constantly show up in all Raman spectra at similar frequencies, but their intensities may vary from one spectrum to another. For instances, the E2-TO + E2-LO peak from the Z-cut sample is much weaker than its equivalents from the X-cut and Y-cut samples whereas the E5-TO + E5-LO peak and E8-TO + E8-LO peak from the Y-cut sample are much weaker than their equivalents from the Z-cut sample. Accordingly, these eight Raman peaks should be most useful in identifying α-quartz.

In addition, there are four doubly degenerated E species, which show clearly separated TO and LO components at relatively lower wavenumbers and higher wavenumbers, respectively (E3-TO and E3-LO, E4-TO and E4-LO, E6-TO and E6-LO, and E7-TO and E7-LO; Fig. 3).

Table 1
Unpolarized Raman features (1300–100 cm^{-1}) of α-quartz with different crystallographic orientations.

Symmetry	Z-cut	X-cut	Y-cut	S1976[a]
A_1-1	207	207	207	207
A_1-2	355	355	356	356
A_1-3	465	465	465	464
A_1-4	1082	1082	1082	1085
E1-TO + E1-LO	128	128	129	128
E2-TO + E2-LO	263	265	265	265
E3-TO	394	394	393	394
E3-LO	–[b]	403	402	401
E4-TO	–[c]	–[c]	449	450
E4-LO	–[b]	509	510	509
E5-TO + E5-LO	695	696	696	697
E6-TO	796	795	795	795
E6-LO	–[b]	808	808	807
E7-TO	1065	1065	1065	1072
E7-LO	–[b]	1230	1231	1231/1235
E8-TO + E8-LO	1161	1160	1159	1162

[a] Scott and Porto [13].
[b] Symmetrically forbidden mode.
[c] Unobserved mode.

The frequencies of the TO components, observed for all three thin sections, remain generally unchanged from one thin section to another, but their intensities may change, being relatively weak from the Y-cut sample but relatively strong from the Z-cut sample. The only exception is the E4-TO peak at ~449 cm^{-1}, which, strongly affected by the adjacent intense A_1-3 peak at ~465 cm^{-1}, is practically very hard to be discerned for all three thin sections hence. In the case of the LO components, both their frequencies and intensities show some variations. As shown in Fig. 3, all the LO components are hardly discernable in the Raman spectrum from the Z-cut sample, and they are stronger in the Raman spectrum from the X-cut sample than from the Y-cut sample. These eight Raman peaks then may cause some complications in interpreting the unpolarized Raman spectra collected from unoriented α-quartz grains.

Summarily, the peak positions of all Raman-active modes of α-quartz revealed by our unpolarized Raman spectra are in excellent agreement with the results in the literature (Table 1) [13,56–58,71], but the peak intensities show some variations.

3.3. Effect of sample thickness on IR absorption spectra

Sample thickness plays a pivotal role in the success of a transmission FTIR measurement. The Beer-Lambert law states that the absorbance A is proportional to the path length of the light through the sample, l (i.e. sample thickness). The intensities of the absorption bands in different energy regions may differ significantly, so that these bands should be probed with thin sections of different thicknesses. For example, the fundamental stretching vibrations of common silicates strongly absorb light and can be successfully detected only with thin sections < ~10 μm thick whereas the combination modes or overtones weakly absorb light and can be readily detected using thin sections with thicknesses up to a few hundreds of microns [48,52]. This is exactly the approach we have adopted in this study.

For α-quartz, its IR absorption intensity in the range of ~1300–650 cm^{-1} (mid-IR region) is extremely strong, and no direct experimental observation has been successful so far [18–20,22,34]. Saksena [34] applied an unpolarized light to his α-quartz thin sections with a minimum thickness of ~31 μm, and observed three IR absorption peaks at ~1235, 1176 and 1047 cm^{-1}, which was rather surprising [20]. Kats [18] used a polarized light to investigate his ~25 μm thick thin section and failed in constraining any IR absorption peaks between ~1250 and 1050 cm^{-1}. Spitzer and Kleinman [19] employed a polarized light to study their ~26 μm thick thin section and revealed a

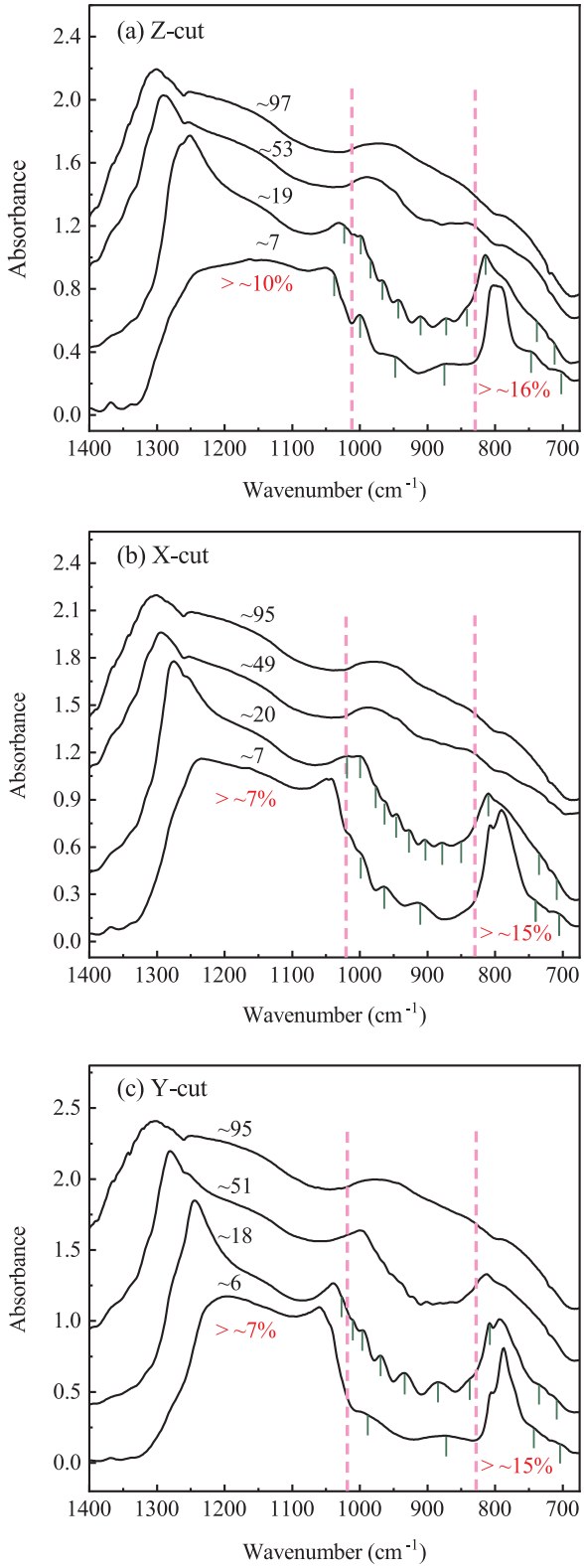

Fig. 4. Unpolarized mid-IR spectra measured from the Z-cut sample (a), the X-cut sample (b), and the Y-cut sample (c). Numbers in black next to the IR spectra are the thicknesses of the thin sections (in μm). Note that reliable infrared peaks, especially in the energy region from ~1300 to 1000 cm^{-1}, emerge only when the sample thickness is reduced to a few microns (~6 μm in the present case), as indicated by the percentages of the transmitted light (numbers in red next to the spectra). The fundamental vibration modes of α-quartz are evidently confined to the energy range < ~1300 cm^{-1}. For the energy range of ~1000–800 cm^{-1}, no fundamental vibration modes appear. The weak peaks at energies > ~1300 cm^{-1} and from ~1000 to 800 cm^{-1} can be attributed as combination bands/overtones, and oscillating interference fringes (tentatively denoted by the short green lines), respectively.

complete absorbance in this energy interval, which confirmed the observation made by Kats [18]. Hanna [20] operated an unpolarized light to examine the ~32 μm thick thin section, and came to the same conclusion. Murray and Gualtieri [22] utilized an unpolarized light to probe their thin section which was less than ~20 μm thick (exact thickness unreported), and found that the IR absorption band at ~1100 cm^{-1} was featureless. As shown in Fig. 4, our experiments clearly demonstrate that only when the sample thickness is reduced to ~6 μm, can these IR absorption peaks in the region of ~1300–1000 cm^{-1} truly express themselves. Another phenomenon is worthy to be pointed out here: when our sample thicknesses are ~100, 50 and 20 μm, interestingly, the transmitted light is always ~3%, which is probably related to some special optical features of α-quartz. Saksena [34] similarly observed a light transmission of ~2–3% for the region of ~1429–1000 cm^{-1} (sample thickness varying from ~114 to 31 μm). The three IR absorption peaks at ~1235, 1176 and 1047 cm^{-1} claimed by him were likely experimental artifacts hence.

Compared to the IR absorption band in the region of ~1300–1000 cm^{-1}, the band at ~800 cm^{-1} is less light-absorbing, so that the corresponding IR absorption peaks should have been much better experimentally-determined. Using polarized lights to probe thin sections of similar thicknesses, Kats (sample thickness being ~25 μm) [18] observed nice IR absorption peaks whereas Spitzer and Kleinman (sample thickness being ~26 μm) [19] demonstrated a zone with fully-absorbed light. In addition, the unpolarized IR absorbance spectra obtained from ~32 μm thick thin section by Hanna [20] exhibited no valid IR signal while those from < ~20 μm thick thin sections by Murray and Gualtieri [22] showed sharp peaks at ~800 cm^{-1}. Our unpolarized IR spectra reveal that the peaks at ~800 cm^{-1} can be confidently resolved only when the sample thickness is reduced to ~6 μm (Fig. 4). If the thickness of the sample is close to ~20 μm, the positions of the IR peaks cannot be easily defined, and a careful deconvolution of the IR spectra is necessary hence (Fig. 4a,b).

Less IR absorption data existed for the IR features of α-quartz at energies below 650 cm^{-1}, and they demonstrated a region at ~450 cm^{-1} which absorbed light as strongly as the IR band at ~800 cm^{-1} [18–20]. Accordingly, the IR absorbance features in this region should be investigated with very thin samples if similar analytical techniques were employed. On the other hand, they have been successfully detected in this study with much thicker samples (thicknesses being ~50 and 100 μm; Fig. 5). The different FTIR spectrometers used for the mid-IR region and far-IR region should be responsible for this difference.

3.4. Influence of interference fringes on IR absorption spectra

Periodic interference fringes may affect the peak positions and relative peak intensities of the transmission IR spectra [42]. The period of the interference fringe ($\Delta\nu$; cm^{-1}) relies on the sample thickness (l; cm) and refractive index (n), as described by the following equation [77]:

$$l = \frac{m}{2n(\nu_1 - \nu_2)} \quad (2)$$

where m is the number of the period in a given wavenumber range between ν_1 and ν_2 (cm^{-1}; ν_1 and ν_2 representing the highest and lowest wavenumbers of the selected interval, respectively). For certain wavenumber range of certain sample, therefore, there is a positive correlation between the l and m. As the sample becomes extremely thick, on one hand, the number of the period will become very large, the period

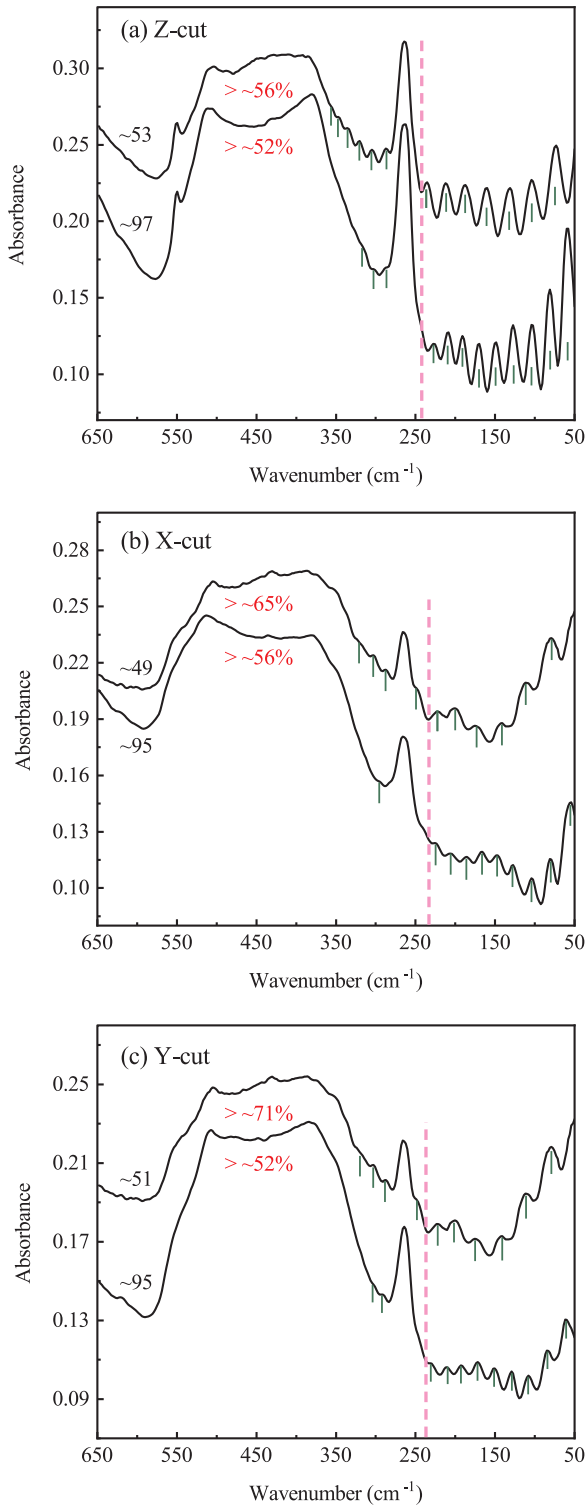

Fig. 5. Unpolarized far-IR spectra measured from the Z-cut sample (a), the X-cut sample (b), and the Y-cut sample (c). Numbers in black next to the IR spectra are the thicknesses of the thin sections (in μm), and numbers in red are the percentages of the transmitted light. The major IR features observed from one thin section with different sample thicknesses are much comparable. The oscillating peaks from ~350 to 50 cm^{-1} can be confidently attributed as interference fringes (denoted by the short green lines). Mainly due to the interaction with the fundamental IR peaks, the anticipated interference fringes at > ~350 cm^{-1} can not be clearly observed, and thus bear large uncertainties. Note that they are more prominent in the spectra collected from the ~50 μm thick thin sections. These very weak peaks at > ~350 cm^{-1} cannot be combination bands/overtones; otherwise, they should be more prominent in the IR spectra collected from the thicker samples.

will be infinitesimal, and eventually no discernable oscillating interference fringes should appear. As the sample becomes extremely thin, on the other hand, the number of the period will become very small, the period will be very large (possibly larger than the wavenumber range ν_1–ν_2), and eventually no oscillating interference fringes could be easily observed as well. In other words, the oscillating interference fringes should mostly occur in the transmission IR spectra collected from samples with appropriate thicknesses.

Oscillating interference fringes were well observed in the transmission IR spectra of α-quartz [18–20,34,78,79], and led to some confusion in the data interpretation. For example, those weak peaks at ~1000, 930, 890 and 852 cm^{-1} found by Kats [18] and at ~1001, 946, 896 and 868 cm^{-1} observed by Hanna [20] were likely interference fringes, and should not be assigned as fundamental vibrational modes. Spitzer and Kleinman [19] addressed the interference fringe issue in the transmission IR spectra of α-quartz, which was useful in interpreting the data (especially informative for the data range with a high light transmission).

In this study, oscillating interference fringes are clearly observed for several energy intervals with high levels of light transmission (Figs. 4 and 5). In the energy range of ~1010–830 cm^{-1}, ~7 weak peaks were detected for the ~20 μm thick samples whereas ~3 weak peaks were found for the ~7 μm thick samples, generally meeting the requirement of Eq. (2). The thicknesses of ~50 and 100 μm seem too thick, and the corresponding transmission IR spectra consequently do not show any compelling evidence to the presence of oscillating interference fringes. The oscillating interference fringes displayed by the ~20 and ~7 μm thick samples cannot be assigned as combination bands or overtones. If they were combination bands or overtones, they would have been more clearly observed in the transmission IR spectra collected from the ~100 and 50 μm thick thin sections. Apparently this is not the case (Fig. 4).

Prominent oscillating interference fringes are also observed in the range of ~250–50 cm^{-1} of our transmission far-IR spectra collected from the ~100 and 50 μm thick thin sections (Fig. 5), in good agreement with Hanna [20], Russell and Bell [80], Bréhat and Wyncke [78], and Wyncke et al. [79]. The thickness of the former samples is about 1.9 times of the thickness of the latter samples, and the number of its weak peaks (~9) is approximately 1.5 times of the number of the weak peaks of the latter (~6), broadly in accordance with Eq. (2).

How the interference fringes interact with the IR absorbance features of α-quartz is by no means simple. When an IR absorbance peak is approached, the refractive index (n) increases dramatically [19,33,78–80], and the number of the interference fringes is thus expected to increase as well (Eq. (2)). In comparison to the monotonic dependence of the refractive index on the wavenumber in the low absorbing regions, the correlation between these two variables in the high absorbing regions where the IR absorbance peaks occur is strongly asymmetric and hardly describable by any simple algorithm. Furthermore, the properties of the interference fringes such as the peak width and peak intensity may vary with the wavenumber. It is then very difficult to confidently detect the interference fringes in the high absorbing regions, which consequently prevents precisely removing their influence from the IR absorption spectra.

Our IR absorption spectra of α-quartz appear as platforms in the regions of ~1300–1000 cm^{-1} (Fig. 4) and 550–350 cm^{-1} (Fig. 5). Although no evident oscillating weak peaks can be clearly observed, it is believed that the interference fringes may have made their contributions. How to get rid of their influence, large or small, is indubitably a challenging task.

3.5. Deconvolution of IR absorption spectra

One particular difficulty arising in the transmission FTIR spectra of α-quartz is that the peaks are not well separated, especially for the energy ranges of ~1300–1000 cm^{-1} (Fig. 4) and ~550–300 cm^{-1} (Fig. 5). This reflects the fact that the SiO_4 tetrahedra in α-quartz are

fully polymerized into a framework [16], completely different from the isolated SiO_4 groups in some minerals like olivine [81] and garnet [82]. The interference fringes further exacerbate the situation, as discussed above. As such, it is very difficult to accurately extract the information of the fundamental IR absorption peaks from the experimental IR data. Fortunately there have been adequate Raman data, and single-crystal IR emission, IR reflection, and IR absorption data, which generally constrain the frequencies of the fundamental IR absorption peaks of α-quartz. During our spectrum-deconvolution process, consequently, we first add some intense IR absorption peaks at frequencies expected for certain fundamental IR vibrational modes, and then add tentatively some weak interference peaks at regions where obvious differences exist between the experimental IR curve and calculated IR curve. The information of these peaks (Gaussian-Lorentzian form) was eventually employed to reproduce the experimentally-obtained IR spectra using the PeakFit V4.12 software (SPCC Inc.). It should be pointed out that the introduction of some interference peaks in the high absorbing regions is more or less arbitrary, potentially leading to some uncertainties in our final results.

3.5.1. The ~1300–1000 cm^{-1} energy region

The unpolarized single-crystal IR absorption spectra taken on the Z-cut, X-cut and Y-cut samples with the thickness of ~6 μm have been deconvoluted (Fig. 6), with the results presented in Table 2.

For the Z-cut sample, the fundamental vibrational modes of the A_2-4-LO, *E*8-TO and *E*7-TO are expected to appear at ~1240, 1163 and 1065 cm^{-1}, respectively (Table 1) [19,65]. Indeed, we have found them at corresponding frequencies of ~1249, 1163 and 1067 cm^{-1} (Fig. 6a). In detail, the frequency of the A_2-4-LO mode seems slightly larger than most early determinations, but in good agreement with the result obtained from the IR ellipsometric spectra of α-quartz (1248.5 cm^{-1}) [41]. Furthermore, the frequency of the *E*7-TO and *E*8-TO mode constrained here are in excellent agreement not only with most early determinations, but with the result acquired from the IR ellipsometric spectra of α-quartz as well (~1065 and 1161 cm^{-1}) [41]. The IR ellipsometric spectrum is an elegant and efficient technique which can obtain simultaneously both absorptive and dispersive parts of the optical response of certain vibrational mode, so that both the TO and LO components along the optical axis and perpendicular to it can be well probed [41].

For the X-cut sample, the fundamental vibrational modes of the A_2-4-TO, *E*7-LO, *E*8-LO + *E*8-TO (negligible peak-splitting, < ~4.5 cm^{-1}) [41], and *E*7-TO are expected to appear at ~1080, 1230, 1163, and 1065 cm^{-1}, respectively (Table 1) [65]. We have correspondingly located them at ~1084, 1241, 1162, and 1057 cm^{-1} (Fig. 6b). These normal modes should also be present in the unpolarized IR absorption spectrum taken from the Y-cut sample, and they have been detected at frequencies of ~1085, 1230, 1162, and 1057 cm^{-1}, as shown in Fig. 6c. Evidently the frequencies of these vibrational modes determined from the X-cut sample and Y-cut sample are identical within experimental uncertainties.

Directly from our single-crystal IR absorption spectra, the extremely high absorbing vibrational modes of α-quartz in the ~1300–1000 cm^{-1} energy region have been successfully extracted. It should be emphasized that this has never been achieved before.

3.5.2. The ~850–675 cm^{-1} energy region

The unpolarized single-crystal IR absorption spectra taken on the Z-cut, X-cut and Y-cut samples with the thickness of ~6 μm have been deconvoluted (Fig. 7), with the results presented in Table 2. In general the IR features in this energy region are sharper, and much better separated than those in the ~1300–1000 cm^{-1} energy region (Fig. 4) and those in the ~550–300 cm^{-1} energy region (Fig. 5), so that higher accuracies in the resulting peak frequencies are expected.

For the Z-cut sample, the fundamental vibrational modes of the A_2-3-LO, *E*6-TO and *E*5-TO are expected to appear at ~790, 797 and 696 cm^{-1}, respectively (Table 1) [13,21,41,65]. Indeed, we have detected them at corresponding frequencies of ~787, 801 and 705 cm^{-1} (Fig. 7a). The absorbance peak at ~705 cm^{-1}, which has been attributed to the *E*5-TO mode here, is extremely weak, and thus cannot be entirely ruled out as an interference fringe. Nevertheless, all previous studies have suggested that the *E*5-TO mode should appear as an extremely weak IR peak [26,27,65].

For the X-cut sample, the fundamental vibrational modes of the A_2-3-TO, *E*6-LO, *E*6-TO, and *E*5-LO + *E*5-TO (negligible peak-splitting, < ~2.5 cm^{-1}) [41] are expected to occur at ~777, 808, 797, and 696 cm^{-1}, respectively (Table 1) [13,21,41,65]. We have correspondingly located them at ~774, 809, 791, and 706 cm^{-1} (Fig. 7b). These

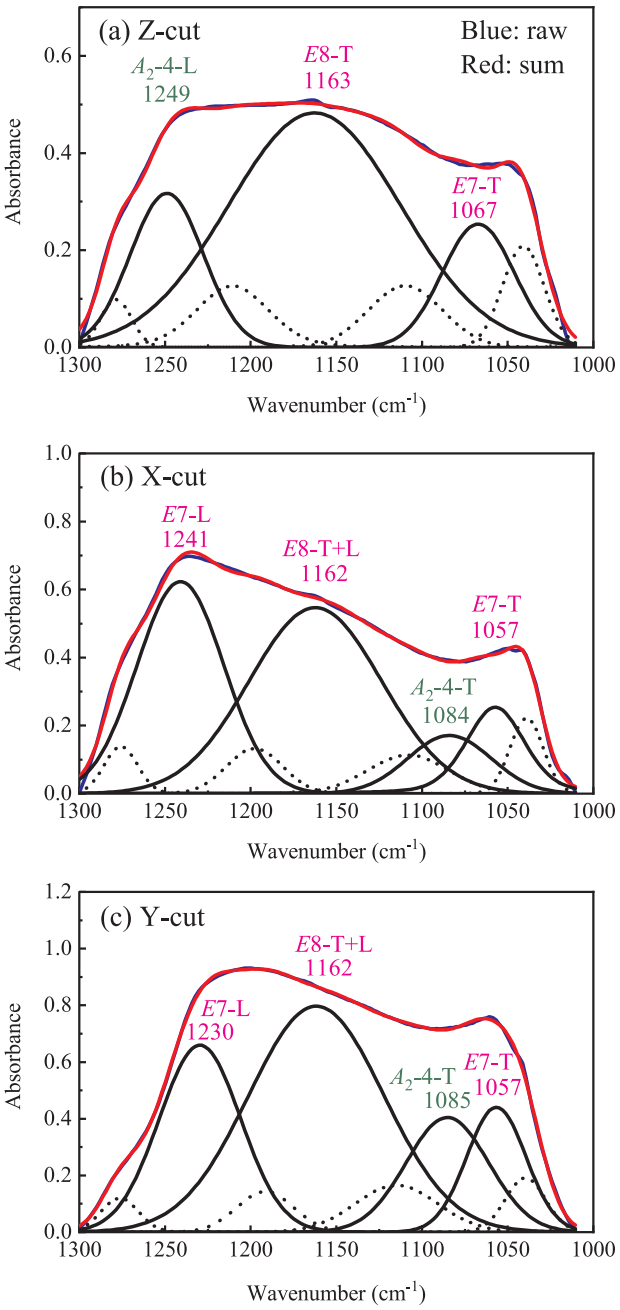

Fig. 6. Gaussian-Lorentzian deconvolution of the mid-IR absorbance spectra in the ~1300–1000 cm^{-1} region taken on the ~6 μm thick thin sections of the Z-cut sample (a), the X-cut sample (b), and the Y-cut sample (c). The sum (the red curve) of the fundamental absorption peaks (the black solid curves) and the interference peaks (the black dotted curves) agrees well with the raw data (the blue curve; baseline correction performed) for the entire data range.

Table 2
Fundamental IR absorption features (1300–675 cm^{-1}) of α-quartz with different crystallographic orientations at ambient conditions.

Symmetry	Z-cut			X-cut			Y-cut		
	Peak	Intensity	FWHM	Peak	Intensity	FWHM	Peak	Intensity	FWHM
*A*2-3-TO	–[a]	–	–	774	0.30(27)[b]	25(11)	772	0.03(2)	23(5)
*A*2-3-LO	787	0.29(9)	22(2)	–[a]	–	–	–[a]	–	–
*A*2-4-TO	–[a]	–	–	1084	0.2(1451)	57(5741)	1085	0.4(375)	57(1454)
*A*2-4-LO	1249	0.32(134)	50(84)	–[a]	–	–	–[a]	–	–
*E*5-TO	705	0.04(1)	19(3)	706	0.05(3)	21(7)	706	0.09(1)	21(1)
*E*5-LO	–[a]	–	–	706	0.05(3)	21(7)	706	0.09(1)	21(1)
*E*6-TO	801	0.38(3)	27(3)	791	0.47(28)	21(6)	788	0.58(4)	18(1)
*E*6-LO	–[a]	–	–	809	0.49(8)	21(1)	807	0.28(2)	14(1)
*E*7-TO	1067	0.25(82)	50(115)	1057	0.25(678)	40(273)	1057	0.4(228)	41(409)
*E*7-LO	–[a]	–	–	1241	0.62(589)	60(127)	1230	0.7(109)	56(160)
*E*8-TO	1163	0.48(44)	118(531)	1162	0.55(347)	91(2201)	1162	0.80(721)	93(1939)
*E*8-LO	–[a]	–	–	1162	0.55(347)	91(2201)	1162	0.80(721)	93(1939)

[a] Symmetrically forbidden mode.
[b] Number in the parenthesis representing one standard deviation; 0.30(27) read as 0.30 ± 0.27.

normal modes should also be present in the unpolarized IR absorption spectrum taken from the Y-cut sample, and they have been detected at frequencies of ~772, 807, 788, and 706 cm^{-1}, as shown in Fig. 7c.

With the exceptions of the fundamental vibrational modes *E*5-LO and *E*5-TO, summarily, all the rest modes appearing in the ~850–675 cm^{-1} energy region have been accurately constrained by our unpolarized IR absorption data (Fig. 7). The frequencies of the weakly light-absorbing *E*5-LO and *E*5-TO modes are slightly larger than most early determinations (by ~8 cm^{-1}), which raises the question whether the IR features at ~705 cm^{-1} belong to the *E*5-LO and *E*5-TO modes or not. As discussed before, they could be just interference fringes, alternatively. The discrepancies between this study and the rest are still within the experimental uncertainties though (e.g. experimental uncertainty up to ~16 cm^{-1} in Spitzer and Kleinman [19]).

3.5.3. The ~550–250 cm^{-1} energy region

The unpolarized single-crystal far-IR absorption spectra taken on the Z-cut, X-cut and Y-cut samples with a thickness of ~100 μm have been deconvoluted (Fig. 8), with the results presented in Table 3.

For the Z-cut sample, the fundamental vibrational modes of A_2-2-LO, A_2-1-LO, *E*4-TO, *E*3-TO and *E*2-TO should occur at ~547, 388, 450, 394 and 265 cm^{-1}, respectively (Table 1) [13,21,65]. Indeed, we have detected them at corresponding frequencies of ~550, 376, 463, 399 and 265 cm^{-1} (Fig. 8a). Although its intensity is low, the absorbance peak at ~550 cm^{-1} can be confidently attributed to the A_2-2-LO mode here, in good agreement with previous investigations [41,54].

For the X-cut sample, the fundamental vibrational modes of A_2-2-TO, A_2-1-TO, *E*4-LO, *E*4-TO, *E*3-LO, *E*3-TO, and *E*2-LO + *E*2-TO (negligible peak-splitting, < ~2 cm^{-1}) are expected to appear at ~489, 364, 510, 450, 403, 394, and 265 cm^{-1}, respectively (Table 1) [13,29,65]. We have correspondingly located them at ~492, 356, 520, 447, 405, 378, and 265 cm^{-1} (Fig. 8b). These normal modes should also be present in the unpolarized IR absorption spectrum taken from the Y-cut sample, and they have been detected at frequencies of ~491, 351, 516, 445, 403, 377, and 265 cm^{-1}, as shown in Fig. 8c.

The *E*3-TO mode has been well located at ~394 cm^{-1} by our unpolarized Raman spectra (Table 1) and by early single-crystal IR reflection data [19]. It is observed at ~399 cm^{-1} with our unpolarized IR absorbance spectrum from the Z-cut sample, but at ~377 cm^{-1} with our spectrum from either the X-cut or Y-cut sample (Table 3). This large discrepancy might represent the maximum uncertainty in determining the frequencies of the fundamental modes of α-quartz with the present experimental protocol. With the exception of the *E*4-TO mode, all other fundamental IR vibrational modes show considerably smaller differences among the frequencies extracted from the unpolarized IR absorption spectra taken on thin sections with different orientations (Tables 2 and 3).

3.5.4. The energy region < ~250 cm^{-1}

For this region, one extremely weak IR absorption peak which contains two components of *E*1-LO and *E*1-TO is expected to occur at ~128 cm^{-1} (Table 1) [78,80,83]. The TO-LO splitting of the *E*1 mode is extremely small, and can be observed only under nonhydrostatic conditions [58,66]. From an X-cut sample as thick as ~265 μm, this peak was vaguely observed by Bréhat and Wyncke [78] using an incident light polarized perpendicularly to the optical axis, but was not observed by Wyncke et al. [79] using an incident light polarized parallel to the optical axis. All our thin sections are too thin to allow any confident detection of this IR feature (Fig. 5), in good agreement with all existing studies.

4. Discussion

Because of the importance of the vibrational features of α-quartz, Raman spectroscopy, emission IR spectroscopy, reflection IR spectroscopy and absorption IR spectroscopy have been employed to ascertain the frequencies of its fundamental vibrational modes (Tables 1 and 4). Simulations have also been performed. Despite all these efforts, however, significant discrepancies existed, particularly for those strong light-absorbing vibrational modes in the energy ranges of ~1300–1000 cm^{-1}, 850–675 cm^{-1} and 550–300 cm^{-1}. One of the major reasons behind was that nearly all intense fundamental IR-active modes of α-quartz have never been directly observed by single-crystal absorption IR spectra due to the difficulty in preparing super thin sample plates.

Via preparing oriented thin sections with the thicknesses ranging down to ~6 μm, we have successfully collected the single-crystal unpolarized absorption IR spectra for those strong light-absorbing regions of α-quartz, and directly constrained the frequencies of all four A_2 modes and seven *E* modes (with the only *E* mode at ~128 cm^{-1} unobserved; Figs. 6–8). Further, the TO and LO components of these modes have been determined. Combining the results gained in this study with the knowledge about the *E* mode at ~128 cm^{-1} in the literature, we have eventually arrived at a full set of frequency data for all those fundamental IR-active modes of α-quartz (Table 4), which seems well consistent with the results obtained by the single-crystal emission IR spectroscopy, single-crystal reflection IR spectroscopy and theoretical simulations. In spite of similar experimental techniques employed, however, large differences between this study and Saksena [34] exist for the fundamental vibrational modes in the energy range of ~1300–1000 cm^{-1}. It is believed that the results from Saksena [34] were subject to large errors caused by complete light-absorbing, as pointed out by Spitzer and Kleinman [19]. Furthermore, the frequencies of α-quartz acquired by the powder IR spectroscopic method are very different to those derived by all other methods, suggesting that this

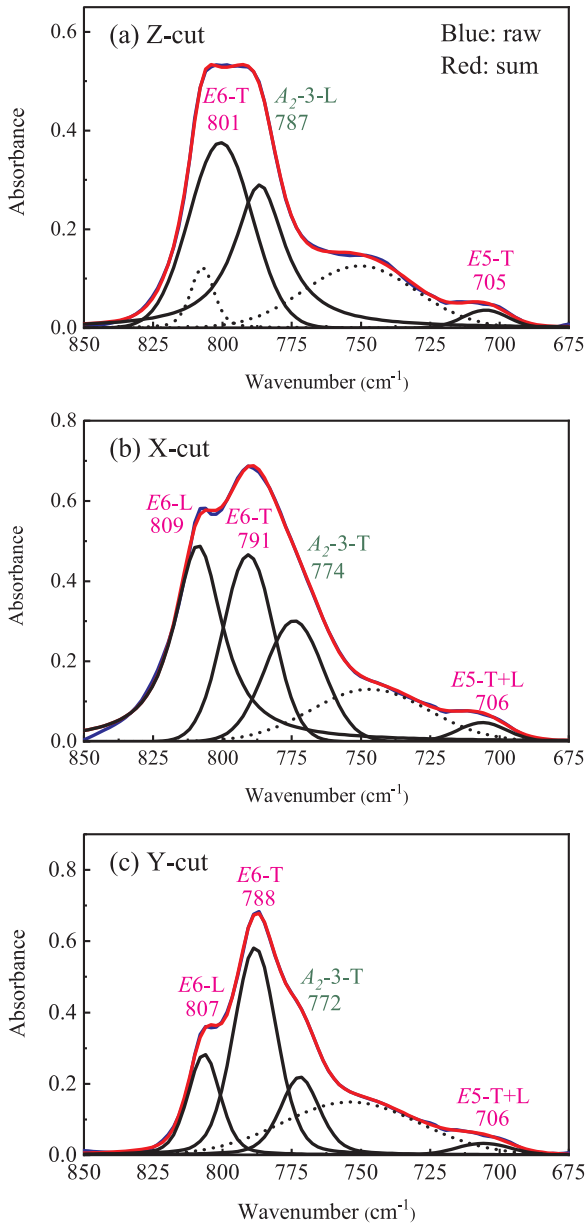

Fig. 7. Gaussian-Lorentzian deconvolution of the mid-IR absorbance spectra in the ~850–675 cm^{-1} region taken on the ~6 μm thick thin sections of the Z-cut sample (a), the X-cut sample (b), and the Y-cut sample (c). The sum (the red curve) of the fundamental absorption peaks (the black solid curves) and the interference peaks (the black dotted curves) agrees well with the raw data (the blue curve; baseline correction performed) for the entire data range.

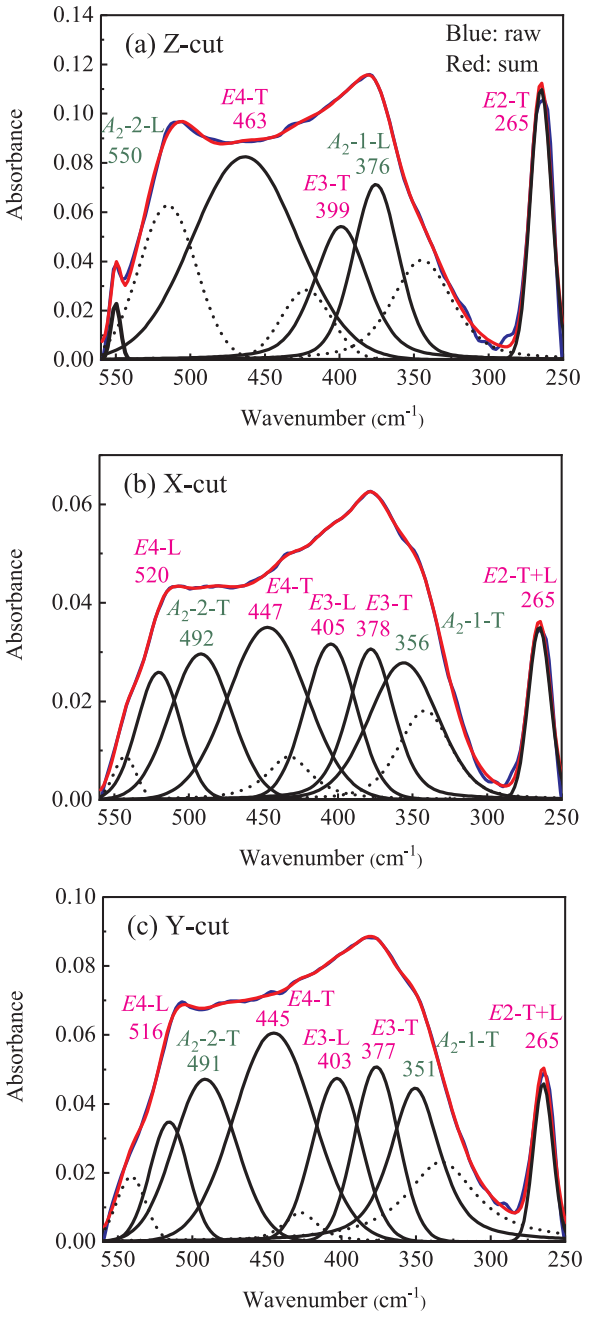

Fig. 8. Gaussian-Lorentzian deconvolution of the far-IR absorbance spectra in the ~550–250 cm^{-1} region taken on the ~100 μm thick thin sections of the Z-cut sample (a), the X-cut sample (b), and the Y-cut sample (c). The sum (the red curve) of the fundamental absorption peaks (the black solid curves) and the interference peaks (the black dotted curves) agrees well with the raw data (the blue curve; baseline correction performed) for the most data range. Some small differences are found at ~300 cm^{-1}, where no fundamental absorption peaks are expected for α-quartz.

experimental technique might be useful in phase-identifying, but is unable to reveal the intrinsic properties of the fundamental vibrational modes (Table 4).

The frequencies of the fundamental vibrational modes extracted from our single-crystal unpolarized absorption IR spectra might bear some uncertainties, which are hard to gauge at the present. The interference fringes should be the primary contributor to these uncertainties. Unfortunately, the nature of the interaction between the strong light-absorbing IR peaks and the weak interference fringes has not been understood. According to Eq. (2), for example, more interference fringes are expected for the regions, where the strong IR absorption peaks occur and accompany sharp increases of the refractive index [33], than for the regions with strong light transmission. However, our spectrum-deconvolution process requires at most 4 additional interference fringe peaks in the 1300–1000 cm^{-1} region (Fig. 6), 2 in the ~850–675 cm^{-1} region (Fig. 7) and 3 in the 550–250 cm^{-1} region (Fig. 8), which does not meet the expectation. Alternatively, it is highly possible that intense interference might not take place in the strong light-absorbing regions since most light should have been absorbed by the material under investigation. If this is the case, the frequencies of the fundamental IR vibrational modes constrained in this study should be accurate.

The intensities and full-widths at half maximums (FWHM) of the fundamental IR-active vibrational modes determined in this study bear large uncertainties (Tables 2 and 3). Mainly due to the characteristic

Table 3
Fundamental IR absorption features (600–100 cm^{-1}) of α-quartz with different crystallographic orientations at ambient conditions.

Symmetry	Z-cut			X-cut			Y-cut		
	Peak	Intensity	FWHM	Peak	Intensity	FWHM	Peak	Intensity	FWHM
A_2-1-TO	–[a]	–	–	356	0.03(60)[b]	55(310)	351	0.04(17)	39(85)
A_2-1-LO	376	0.07(36)	36(103)	–[a]	–	–	–[a]	–	–
A_2-2-TO	–[a]	–	–	492	0.03(165)	48(1298)	491	0.05(410)	49(1770)
A_2-2-LO	550	0.02(1)	7(1)	–[a]	–	–	–[a]	–	–
E1-TO	–[c]	–	–	–[c]	–	–	–[c]	–	–
E1-LO	–[a]	–	–	–[c]	–	–	–[c]	–	–
E2-TO	265	0.11(1)	17(1)	265	0.04(0)	17(1)	265	0.05(0)	15(1)
E2-LO	–[a]	–	–	265	0.04(0)	17(1)	265	0.05(0)	15(1)
E3-TO	399	0.05(37)	42(206)	378	0.03(83)	36(538)	377	0.05(61)	35(139)
E3-LO	–[a]	–	–	405	0.03(142)	40(523)	403	0.05(230)	39(365)
E4-TO	463	0.08(7)	83(336)	447	0.04(75)	62(2754)	445	0.06(166)	63(4098)
E4-LO	–[a]	–	–	520	0.03(71)	34(171)	516	0.03(117)	30(168)

[a] Symmetrically forbidden mode.
[b] Number in the parenthesis representing one standard deviation; 0.03(60) read as 0.03 ± 0.60.
[c] Unobserved mode.

framework structure of α-quartz, the IR peaks, especially those in the 1300–1000 cm^{-1} region (Fig. 6) and those in the 550–250 cm^{-1} region (Fig. 8), are not well separated but form platforms, which makes the spectrum-deconvolution process somehow uncertain. It would be nice to compare our experimental data to some theoretical results. Dowty [84], Ocaña et al. [37], and Liang et al. [85] attempted simulating the IR powder spectrum of α-quartz, and Spitzer and Kleinman [19] theoretically reproduced their polarized absorption IR spectra collected from a ~26 μm thick X-cut sample. Since the experimental data were usually used as key references in these calculations, the theoretical results were not fully independent, so that a critical and practical comparison between our experimental results and those from the theoretical investigations is not very meaningful.

5. Conclusions

Transmission FTIR investigation on oriented single crystal is a potent analytical technique to probe the fundamental IR absorption features of α-quartz. Taking into account the influence of sample thickness, unpolarized single-crystal absorption IR spectra have been successfully acquired from the Z-cut sample, the X-cut sample and the Y-cut sample. By resorting to the symmetry analysis and relevant knowledge in the literature, the interference effect has been tentatively removed, and optimal spectroscopic results have been obtained for the fundamental

Table 4
Comparison of fundamental IR features (cm^{-1}) of α-quartz, determined by different experimental and theoretical techniques.

Symmetry	Calculation		Emission	Reflection					Absorption								
									Powder				Single crystal				
	I1976[a]	Z2004	W1996	S1961	G1975	H1994	W1997	P2016	W1986	O1987	W1993	K2013	S1958	K1961	H1965	M1989	TS
A_2-1-TO	368	352	364[b]	364[b]	364	–	357	–	–	374	–	372	–	–	343	355	354
A_2-1-LO	370	377	–	–	387	–	383	–	–	–	–	–	–	–	–	–	376
A_2-2-TO	475	501	494[b]	495[b]	495	495	488	500	–	515	512	515	–	496[b]	–	499	492
A_2-2-LO	524	556	–	539[b]	552	552	543	550	–	–	–	–	–	–	548	–	550
A_2-3-TO	761	784	776[b]	778[b]	777	776	–	780	778[b]	780	780	781	775	766[b]	–	783	773
A_2-3-LO	785	797	–	–	790	789	–	790	–	–	–	–	–	787[b]	–	–	787
A_2-4-TO	1088	1076	1074[b]	1080[b]	1071	1073	–	1070	1145	1150	1080	–	–	–	–	1243?	1084
A_2-4-LO	1245	1252	1215[b]	1227[b]	1229	1249	–	1230	–	–	–	–	–	–	–	–	1249
E1-TO	127	132	–	–	–	–	132	–	–	–	–	128?	–	–	138	133	–
E1-LO	129	133	–	–	–	–	132	–	–	–	–	–	–	–	–	–	–
E2-TO	255	264	–	–	–	–	263	–	–	–	–	264	–	–	262	276	265
E2-LO	272	266	–	–	–	–	265	–	–	–	–	–	–	–	–	–	265
E3-TO	377	391	393[b]	394[b]	394	–	384	400	–	398	–	397	–	–	394	407	399
E3-LO	390	400	–	–	402	–	398	–	–	–	–	–	–	–	–	–	404
E4-TO	485	447	449[b]	450[b]	450	450	444	–	–	470	458	465	–	460[b]	468	475	463
E4-LO	553	508	509[b]	509[b]	510	508	502	–	–	–	–	–	–	496[b]	–	–	518
E5-TO	730	703	694[b]	697[b]	695	695	–	696	695	697	696	694	695	695[b]	695?	690	706
E5-LO	730	706	–	–	698	698	–	–	–	–	–	–	–	–	–	–	706
E6-TO	794	811	795[b]	797[b]	797	795	–	800	801[b]	800	800	800	787	787[b]	797	813	790
E6-LO	826	823	–	–	810	809	–	–	–	–	–	–	812	812[b]	–	–	808
E7-TO	1078	1068	1067[b]	1072[b]	1065	1065	–	1060	1085[b]	1095	–	1093	1047?	–	–	1133?	1067
E7-LO	1225	1243	1222[b]	1220[b]	1226	1239	–	1250	–	–	–	–	1235?	–	–	–	1235
E8-TO	1153	1163	1161[b]	1163[b]	1158	1161	–	1160	1175	1170	1170	1168	1176?	–	–	1237?	1162
E8-LO	1147	1160	–	–	1155	1158	–	–	–	–	–	–	–	–	–	–	1162

[a] Data source: I1976, Iishi (a polarizable ion model) [14]; Z2004, Zicovich-Wilson et al. (a hybrid B3LYP Hamiltonian) [31]; W1996, Wenrich and Christensen [23]; S1961, Spitzer and Kleinman [19]; G1975, Gervais and Piriou [21]; W1997, Wyncke et al. [79]; P2016, Pellicer-Porres et al. [86]; H1994, Humlíček [41]; W1986, Wong et al. [36]; O1987, Ocaña et al. [37]; W1993, Williams et al. [87]; K2013, Koike et al. [24]; S1958, Saksena [34]; K1961, Kats [18]; H1965, Hanna [20]; M1989, Murray and Gualtieri [22]; TS, This study.
[b] Reassigned mode on the basis of symmetry analysis.

IR-active modes, leading to a full description of the vibrational features of α-quartz. Especially, the present contribution made the effort preparing super thin samples (~6 μm thick), which enabled a direct observation of those strong light-absorbing IR peaks in the 1300–1000 cm^{-1} region. This practice removed many ambiguities and even mistakes in previous IR data of α-quartz. The full description of the vibrational features of α-quartz derived in this study will play an important role in further theoretical calculations, and lead to better understanding of the structural and vibrational features of α-quartz, its polymorphs, amorphous silica, and even other silicate minerals.

Acknowledgements

This study was financially supported by the Program of the Data Integration and Standardization in the Geological Science and Technology from MOST, China (Grant No. 2013FY1109000-3), by the DREAM project of MOST, China (Grant No. 2016YFC0600408), and by the Strategic Priority Research Program (B) of Chinese Academy of Sciences (Grant No. XDB18000000).

References

[1] A.B. Ronov, A.A. Yaroshevsky, P.J. Hart (Ed.), The Earth's Crust and Upper Mantle, AGU, Washington, 1969, pp. 37–57.
[2] J. Götze, R. Möckel, Quartz: Deposits, Mineralogy and Analytics, Springer, Berlin/Heidelberg, 2012.
[3] A. Wang, L.A. Haskin, E. Cortez, Appl. Spectrosc. 52 (1998) 477–487, https://doi.org/10.1366/0003702981943842.
[4] A.M. Hofmeister, A. Chopelas, Phys. Chem. Miner. 17 (1991) 503–526, https://doi.org/10.1007/BF00202230.
[5] A.M. Hofmeister, P.A. Giesting, B. Wopenka, G.D. Gwanmesia, B.L. Jolliff, Am. Mineral. 89 (2004) 132–146, https://doi.org/10.2138/am-2004-0116.
[6] A.M. Hofmeister, K.M. Pitman, Phys. Chem. Miner. 34 (2007) 319–333, https://doi.org/10.1007/s00269-007-0150-1.
[7] R.C. Lord, J.C. Morrow, J. Chem. Phys. 26 (1957) 230–232, https://doi.org/10.1063/1.1743274.
[8] S.W. Kieffer, Rev. Geophys. 17 (1979) 20–34, https://doi.org/10.1029/RG017i001p00020.
[9] S.W. Kieffer, Rev. Geophys. 17 (1979) 35–59, https://doi.org/10.1029/RG017i001p00035.
[10] P.F. McMillan, A.N. Lazarev, S.W. Kieffer, V.M. Agoshkov, G. Buntebarth, A. Gliko, A.S. Marfunin (Ed.), Advanced Mineralogy, Springer, Berlin, 1994, pp. 412–435.
[11] A.M. Hofmeister, Am. Mineral. 86 (2001) 1188–1208, https://doi.org/10.2138/am-2001-1008.
[12] A.M. Hofmeister, H.K. Mao, Am. Mineral. 86 (2001) 622–639, https://doi.org/10.2138/am-2001-5-604.
[13] J.F. Scott, S.P.S. Porto, Phys. Rev. 161 (1967) 903–910, https://doi.org/10.1103/PhysRev.161.903.
[14] K. Iishi, Z. Kristallogr. 144 (1976) 289–303, https://doi.org/10.1524/zkri.1976.144.1-6.289.
[15] P.F. McMillan, A.C. Hess, Phys. Chem. Miner. 17 (1990) 97–107, https://doi.org/10.1007/BF00199660.
[16] J.D. Dana, E.S. Dana, C. Frondel, Silica Materials, Wiley, New York, 1962.
[17] L.P. Davila, S.H. Risbud, J.F. Shackelford, J.F. Shackelford, R.H. Doremus (Eds.), Ceramic and Glass Materials: Structure, Properties and Processing, Springer, Boston, 2008, pp. 71–86.
[18] A. Kats, Hydrogen in Alpha Quartz, PhD dissertation Delft University of Technology, Netherland, 1961.
[19] W.G. Spitzer, D.A. Kleinman, Phys. Rev. 121 (1961) 1324–1335, https://doi.org/10.1103/PhysRev.121.1324.
[20] R. Hanna, J. Am. Ceram. Soc. 48 (1965) 595–599, https://doi.org/10.1111/j.1151-2916.1965.tb14680.x.
[21] F. Gervais, B. Piriou, Phys. Rev. B 11 (1975) 3944–3950, https://doi.org/10.1103/PhysRevB.11.3944.
[22] R.A. Murray, J.G. Gualtieri, Proc. 43rd Annu. Symp. Freq. Control. (1989) 477–484, https://doi.org/10.1109/FREQ.1989.68906.
[23] M.L. Wenrich, P.R. Christensen, J. Geophys. Res. 101 (1996) 15921–15931, https://doi.org/10.1029/96JB01153.
[24] C. Koike, R. Noguchi, H. Chihara, H. Suto, O. Ohtaka, Y. Imai, T. Matsumoto, A. Tsuchiyama, Astrophys. J. 778 (2013) 60, https://doi.org/10.1088/0004-637X/778/1/60.
[25] C.J. Hardgrove, A.D. Rogers, T.D. Glotch, J.A. Arnold, J. Geophys. Res. Planets 121 (2016) 542–555, https://doi.org/10.1002/2015JE004919.
[26] J. Etchepare, M. Merian, L. Smetankine, J. Chem. Phys. 60 (1974) 1873–1876, https://doi.org/10.1063/1.1681287.
[27] K. Iishi, K.H. Yamaguchi, Am. Mineral. 60 (1975) 907–912.
[28] K. Iishi, Am. Mineral. 63 (1978) 1190–1197, https://doi.org/10.1103/PhysRevLett.78.2413.
[29] X. Gonze, D.C. Allan, M.P. Teter, Phys. Rev. Lett. 68 (1992) 3603–3606, https://doi.org/10.1103/PhysRevLett.68.3603.
[30] P. Umari, A. Pasquarello, A.D. Corso, Phys. Rev. B 63 (2001) 094305, , https://doi.org/10.1103/PhysRevB.63.094305.
[31] C.M. Zicovich-Wilson, F. Pascale, C. Roetti, V.R. Saunders, R. Orlando, R. Dovesi, J. Comput. Chem. 25 (2004) 1873–1881, https://doi.org/10.1002/jcc.20120.
[32] K. Refson, P.R. Tulip, S.J. Clark, Phys. Rev. B 73 (2006) 155114, , https://doi.org/10.1103/PhysRevB.73.155114.
[33] F. Gangemi, R. Gangemi, A. Carati, A. Maiocchi, L. Galgani, Europhys. Lett. 116 (2016) 37001, https://doi.org/10.1209/0295-5075/116/37001.
[34] B.D. Saksena, Proc. Phys. Soc. Lond. 72 (1958) 9–16, https://doi.org/10.1088/0370-1328/72/1/303.
[35] I.I. Plyusnina, M.N. Maleyev, G.A. Yefimova, Int. Geol. Rev. 13 (1971) 1750–1754, https://doi.org/10.1080/00206817109475637.
[36] P.T.T. Wong, F.L. Baudais, D.J. Moffatt, J. Chem. Phys. 84 (1986) 671–674, https://doi.org/10.1063/1.450563.
[37] M. Ocaña, V. Fornes, J.V. Garcia-Ramos, C.J. Serna, Phys. Chem. Miner. 14 (1987) 527–532, https://doi.org/10.1007/BF00308288.
[38] P.L. King, J.F. Larsen, Am. Mineral. 98 (2013) 1162–1171, https://doi.org/10.2138/am.2013.4277.
[39] M.R.M. Izawa, P.L. King, R.L. Flemming, R.C. Peterson, P.J.A. McCausland, J. Geophys. Res. 115 (2010) E07008, , https://doi.org/10.1029/2009JE003452.
[40] A.M. Hofmeister, E. Keppel, A.K. Speck, Mon. Not. R. Astron. Soc. 345 (2003) 16–38, https://doi.org/10.1046/j.1365-8711.2003.06899.x.
[41] J. Humlíček, Philo. Mag. B 70 (1994) 699–710, https://doi.org/10.1080/01418639408240243.
[42] K. Yamamoto, H. Ishida, Vib. Spectrosc. 8 (1994) 1–36, https://doi.org/10.1016/0924-2031(94)00022-9.
[43] M. Born, K. Huang, Dynamical Theory of Crystal Lattices, Oxford University Press, Oxford, 1964.
[44] G. Andermann, A. Caron, D.A. Dows, J. Opt. Soc. Am. 55 (1965) 1210–1216, https://doi.org/10.1364/JOSA.55.001210.
[45] S.S. Mitra, S. Nudelman, S.S. Mitra (Eds.), Optical Properties of Solids, Plenum Press, New York, 1969, pp. 333–452.
[46] X. Liu, H.St.C. O'Neill, A.J. Berry, J. Petrol. 47 (2006) 409–434, https://doi.org/10.1093/petrology/egi081.
[47] F.W. von Aulock, B.M. Kennedy, C.I. Schipper, J.M. Castro, D.E. Martin, C. Oze, J.M. Watkins, P.J. Wallace, L. Puskar, F. Bégué, A.R.L. Nichols, H. Tuffen, Lithos 206 (2014) 52–64, https://doi.org/10.1016/j.lithos.2014.07.017.
[48] X. Liu, Y. Ma, Q. He, M. He, J. Asian Earth Sci. 148 (2017) 315–323, https://doi.org/10.1016/j.jseaes.2017.03.016.
[49] A.M. Hofmeister, Phys. Chem. Miner. 14 (1987) 499–513, https://doi.org/10.1007/BF00308285.
[50] A.E. Wald, J.W. Salisbury, J. Geophys. Res. 100 (1995) 24665–24675, https://doi.org/10.1029/95JB02400.
[51] S.W. Ruff, P.R. Christensen, P.W. Barbera, D.L. Anderson, J. Geophys. Res. 102 (1997) 14899–14913, https://doi.org/10.1029/97JB00593.
[52] F. Wang, X. Liu, H. Zheng, L. Zhang, Acta Petrol. Sin. 31 (2015) 1891–1900, https://doi.org/10.1016/S0920-5632(95)80040-9.
[53] D.A. Kleinman, W.G. Spitzer, Phys. Rev. 125 (1962) 16–30, https://doi.org/10.1103/PhysRev.125.16.
[54] M.E. Striefler, G.R. Barsch, Phys. Rev. B 12 (1975) 4553–4566, https://doi.org/10.1103/PhysRevB.12.4553.
[55] F. Pascale, C.M. Zicovich-Wilson, F.L. Gejo, B. Civalleri, R. Orlando, R. Dovesi, J. Comput. Chem. 25 (2004) 888–897, https://doi.org/10.1002/jcc.20019.
[56] J.F. Scott, L.E. Cheesman, S.P.S. Porto, Phys. Rev. 162 (1967) 834–840, https://doi.org/10.1103/PhysRev.162.834.
[57] C.Y. She, J.D. Masso, D.F. Edwards, J. Phys. Chem. Solids 32 (1971) 1887–1900, https://doi.org/10.1016/S0022-3697(71)80154-3.
[58] V.J. Tekippe, A.K. Ramdas, S. Rodriguez, Phys. Rev. B 8 (1973) 706–717, https://doi.org/10.1016/0375-9601(71)90115-0.
[59] J. Tang, X. Liu, Z. Xiong, Q. He, S.R. Shieh, H. Wang, Bull. Mineral. Petrol. Geochem. 33 (2014) 289–298, https://doi.org/10.3969/j.issn.1007-2802.2014.03.016.
[60] K.D. Moller, W.G. Rothschild, Far-infrared Spectroscopy, Wiley-Interscience, New York, 1971, pp. 303–324.
[61] D.D.S. Meneses, P. Melin, L. del Campo, L. Cosson, P. Echegut, Infrared Phys. Technol. 69 (2015) 96–101, https://doi.org/10.1016/j.infrared.2015.01.011.
[62] L. Liu, X. Liu, X. Bao, Q. He, W. Yan, Y. Ma, M. He, R. Tao, R. Zou, Minerals 8 (2018) 210, https://doi.org/10.3390/min8050210.
[63] R.E. Gibbs, Proc. R. Soc. 110 (1926) 443–455, https://doi.org/10.1002/bit.21637.
[64] B.D. Saksena, Proc. Ind. Acad. Sci. 12 (1940) 93–139, https://doi.org/10.1007/BF03170730.
[65] M.M. Elcombe, Proc. Phys. Soc. 91 (1967) 947–958, https://doi.org/10.1088/0370-1328/91/4/323.
[66] R.J. Hemley, M.H. Manghnani, Y. Syono (Eds.), High-Pressure Research in Mineral Physics, AGU, Washington, 1987, pp. 347–359.
[67] F. Wooten, Optical Properties of Solids, Academic Press, London, 1972.
[68] K. Yamamoto, A. Masui, Appl. Spectrosc. 50 (1996) 759–763, https://doi.org/10.1366/0003702963905709.
[69] C. Landsberg, L. Mandelstam, Naturwiss 28 (1928) 557–558, https://doi.org/10.1007/BF01506807.
[70] S.M. Shapiro, D.C. O'Shea, H.Z. Cummins, Phys. Rev. Lett. 19 (1967) 361–364, https://doi.org/10.1103/PhysRevLett.19.361.
[71] J.F. Scott, Phys. Rev. Lett. 21 (1968) 907–910, https://doi.org/10.1103/PhysRevLett.21.907.
[72] S.M. Shapiro, J.D. Axe, Phys. Rev. B 6 (1972) 2420–2427, https://doi.org/10.1103/

PhysRevB.6.2420.
[73] P. Gillet, A. Le Cléac'h, M. Madon, J. Geophys. Res. 95 (1990) 21635–21655, https://doi.org/10.1029/JB095iB13p21635.
[74] C.H. Chio, S.K. Sharma, P.G. Lucey, D.W. Muenow, Appl. Spectrosc. 57 (2003) 774–783, https://doi.org/10.1366/000370203322102852.
[75] K. Ye, J.-B. Liou, B. Cong, S. Maruyama, Am. Mineral. 86 (2001) 1151–1155, https://doi.org/10.2138/am-2001-1004.
[76] Z. Lü, L. Zhang, J. Du, K. Bucher, Am. Mineral. 93 (2008) 1845–1850, https://doi.org/10.2138/am.2008.2800.
[77] K. Shinoda, N. Aikawa, Phys. Chem. Miner. 20 (1993) 308–314, https://doi.org/10.1007/BF00215101.
[78] F. Bréhat, B. Wyncke, Int. J. Infrared Milli. 18 (1997) 1663–1679, https://doi.org/10.1007/bf02678278.
[79] B. Wyncke, F. Bréhat, H. Kharroubi, Int. J. Infrared Milli. 18 (1997) 475–489, https://doi.org/10.1007/bf02677934.
[80] E.E. Russell, E.E. Bell, J. Opt. Soc. Am. 57 (1967) 341–348, https://doi.org/10.1364/JOSA.57.000341.
[81] K.R. Rao, S.L. Chaplot, N. Choudhury, S. Ghose, J.M. Hastings, L.M. Corliss, D.L. Price, Phys. Chem. Miner. 16 (1988) 83–97, https://doi.org/10.1007/BF00201334.
[82] M. Merli, A. Callegari, E. Cannillo, F. Caucia, M. Leona, R. Oberti, L. Ungaretti, Eur. J. Mineral. 7 (1995) 1239–1249, https://doi.org/10.1127/ejm/7/6/1239.
[83] J.N. Plendl, L.C. Mansur, A. Hadni, A. Brehat, P. Henry, G. Morlot, F. Naudin, P. Strimer, J. Phys. Chem. Solids 28 (1967) 1589–1597, https://doi.org/10.1016/0022-3697(67)90290-9.
[84] E. Dowty, Phys. Chem. Miner. 14 (1987) 122–138, https://doi.org/10.1007/BF00308216.
[85] Y. Liang, C.R. Miranda, S. Scandolo, J. Chem. Phys. 125 (2006) 194524, , https://doi.org/10.1063/1.2390709.
[86] J. Pellicer-Porres, A. Segura, D. Santamaría-Pérez, J. Appl. Phys. 119 (2016) 055902, , https://doi.org/10.1063/1.4941268.
[87] Q. Williams, R.J. Hemley, M.B. Kruger, R. Jeanloz, J. Geophys. Res. 98 (1993) 22157–22170, https://doi.org/10.1029/93JB02171.